Multimed Tools Appl
https://doi.org/10.1007/s11042-018-6086-2

Multi-scale completed local binary patterns for ulcer detection in wireless capsule endoscopy images

Meryem Souaidi[1] · **Abdelkaher Ait Abdelouahed**[1] · **Mohamed El Ansari**[1]

Received: 25 September 2017 / Revised: 19 April 2018 / Accepted: 1 May 2018

Abstract This paper deals with ulcer abnormalities detection of small bowel, from wireless capsule endoscopy images (WCE). We propose a multi-scale approach based on completed local binary patterns, and laplacian pyramid (MS-CLBP). The proposed approach captures additional information about the magnitude as a robust descriptor against illuminations changes in WCE images. In addition, ulcer detection, was performed using the Green component and Cr components of RGB and YCbCr color spaces, respectively. Using the support vector machine (SVM) classifier, we conduct several experiments on two datasets. The results obtained validate the efficiency of the proposed system with an average accuracy of 95.11 and 93.88% for both datasets. Finally, a comparison with the state of the art methods shows that the proposed method is superior to the other approaches.

Keywords Wireless capsule endoscopy (WCE) · Ulcer regions · Texture analysis · Completed local binary pattern (CLBP) · Laplacian pyramid · Color space

1 Introduction

Nowadays approximately 10% of the people suffer from ulcer diseases. A bit previous research demonstrated that among the causes of peptic ulcer, the use of nonsteroidal anti

✉ Meryem Souaidi
souaidi.meryem@gmail.com

Abdelkaher Ait Abdelouahed
a.abdelkaher@gmail.com

Mohamed El Ansari
melansari@gmail.com

[1] LabSIV, Department of Computer Science, Faculty of Science, Ibn Zohr University, BP 8106, 80000 Agadir, Morocco

Published online: 05 June 2018

inflammatory drugs ulcerations (NSAID) and a dangerous microaerophilic bacterium (bacterium Helicobacter pylori). In the past, the doctors have used the traditional endoscopy to discriminate colonic diseases including ulcer disease. Despite being efficacious for the upper (deodenum, stomach and food pipe) and lower part (colon, terminal ileum) of the GI tract, it can hardly reach the small intestine. Besides, the patients have to go through severe pain which is highly uncomfortable. To overcome these limitations, the wireless capsule endoscopy examination developed by Given Imaging in 2000 was introduced as a great diagnostic tool in assessing gastrointestinal (GI) bleeding, ulcer, Crohn's disease and other abnormalities occurred in the digestive tract [1]. As shown in Fig. 1, the creative endoscopy capsule contains a miniature video camera, light source, batteries, and a radio transmitter. After being swallowed by a patient who has a diet for about 12 h, it is propelled by peristalsis to slowly moves through the GI tract. It records and wirelessly transmit images to a data-recording device attached to the patient's waist. The all process takes about 8 h until its battery runs out. The examination process is a tedious task for enterologists as it's a time-consuming [2, 10]. We talk about more than two hours for physicians to visualize an approximation of 50,000 images for one patient. The manner in which the transmitted images are examined is incompatible with a reliable and economically practical exploration of this new technique. Therefore, it is important to develop a computer-aided detection (CAD) system to dis-burden physicians. Many diseases of GI tract in CE images show spot patterns including ulcer. This abnormality often appears white or light-gray color compared with normal mucosa. Also, The quality of the obtained images from the WCE shows a great degradation due to illumination changes inside the GI tract. All these reasons motivate us to propose an approach, that not only maintains the complete structural information per scale decomposition, but it also captures additional information about the magnitude as a robust descriptor against illuminations changes in WCE images. Many previous studies have focused on small bowel ulcer detection using typical techniques related to colors, textures, and shapes for describing image properties [40]. Some color based methods were introduced in [14, 37]. Ulcer regions are not characterized by a specific color, unlike the other abnormalities of GI tract bleeding, polyp,..). The ulcer regions -except for the color variation- show more or less differences in texture compared to the healthy ones. Thus, many efforts have been reported to texture based methods [27, 38]. The combination of color and

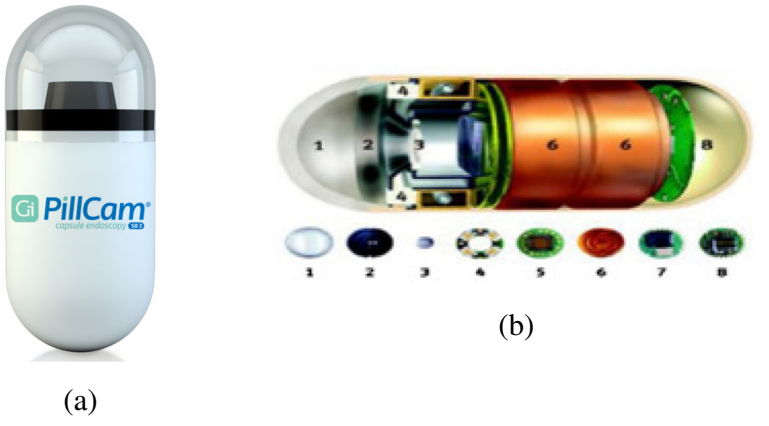

Fig. 1 **b** The components diagram of CE, (1): Optical Dome, (2): lens holder, (3): lens, (4): illuminating source, (5): CMOS image, (6): battery, (7): Transmitter, (8): antenna

texture is presented as whole in a three manner: color channels are operated independently [9, 33]; using the interaction between channels to deal with color texture [5]; color and texture methods are operated separately [36, 39]. Several texture based schemes were proposed to differentiate between normal and ulcer regions in WCE images. Vasileios Charisis, et al. [4] proposed a color-texture method AR-DLac by jointing Bidimensional EMD (BEEMD) analysis to discriminate between ulcer and normal WCE images. Eid et al. [9] presented a curvelet-based lacunarity (DCT-LAC) method in which the lacunarity of each DCT subbands is calculated to extract feature vector from the WCE images. A saliency detection method based on multi-level super pixel representation to discriminate ulcer mucosa in WCE images is presented in [39]. The authors of [17] proposed AdaBoost learning method for ulcer abnormality detection. Based on the efficiency of AdaBoost to outline the distinctive local and global visual features, the authors utilized a simple RGB value as a feature for ulcer discrimination task. An adapted bit planes are used to detect useful areas in ulcer images. Then, two sets of features bit-plane probability and wavelet-based features were extracted from the detected areas and used for classification [32]. Yingju Chen, et al. [6] proposed a method in which a saliency map is created by means of channel mixer to highlight suspicious regions. Once the suspicious region identified, textural features along the contour are extracted and classify them using a trained classifier for ulcer detection. However, local binary pattern and its extended version prove their capabilities as a powerful descriptor in many CAD application. The original LBP and their extended versions proves its efficiency in many applications for ulcer, bleeding and tumor [5, 18, 38]. In [18], authors proposed a curvelet CWC (Color Wavelet covariance) based on local binary pattern (LBP) as a method to extract the texture features. Then, they used MLP classifier in YCbCr color space. Charisis et al. [5], presented an approach that apply at first a color rotation operation (CR) to WCE images before extracting vector feature using the uniform rotation invariant LBP (ULBP). The authors in [38] proposed a bag-of-words model and features fusion technique. The pyramid bag-of-words is applied to LBP and SIFT descriptors to model and describe the image patches. Another study [3] presented a new texture extraction scheme based on local binary pattern variance and discrete wavelet transform for pathological inflammation, polyp, and bleeding regions discrimination in WCE images. The problem is that these methods don't take in consideration the scale information, since the same texture can be visualized as many micro-structural textures at different levels. These reasons have motivated us to proposed in [35] a multi-scale approach based on LBP and Laplacian pyramid transform, to distinguish ulcerous patches from a normal ones. This rotation-and-scale invariant method was applied on the components of four color spaces: RGB, Lab, HSV and CMY to select in the experiments results the best one. This method gained an encouraging results in term of performance, compared to competitive state-of-art methods. Thus, the ulcer abnormality often occur as gray lights or bright spots. These reasons motivate us to use an extended version of LBP (Completed Local Binary Pattern CLBP) which detect also the magnitude of the edge bright spots.

This paper built upon the multi-scale methods based on completed local binary pattern (CLBP) and Laplacian pyramid decomposition. Two variants of MS-CLBP are involved for automatic ulcer disease discrimination in WCE images. The emphasis methods are based on laplacian pyramid in YCbCr and RGB color spaces. The final decision about the most powerful MS-CLBP descriptor is done regarding to their classification accuracy on the experiments. Firstly, we exploit the support vector machine (SVM) [7], random forest (RF) [12, 20], Naive Bayes and K-nearest neighbors (KNN) [30]. Then, the results were promising using the SVM classifier, that's why we report the results obtained with SVM for the comparison with the state-of-art methods. The structure of this paper is organized as

follows.In Section 2 we describe the proposed multi-scale approach, more details about the choice of the color space and the completed LBP are provided too. Experimental results followed by a discussion, are presented in Section 3. Finally, some conclusions end the paper.

2 Proposed method

2.1 The proposed scheme

Texture analysis methods can be categorized into structural, statistical, geometrical, model-based and signal processing methods [13]. Figure 2 illustrates the main steps of the multi-scale approach. Firstly, we consider an input image in a specific color space (RGB or YCbCr). For each component C1, C2 or C3, we applied two completed LBP variants, either $CLBP/M^{ri}_{P,R}$ or $CLBP/S^{ri}_{P,R}$ with a fixing number of LBP neighbors P = 8 and radius R = 1. The resulting completed LBP coded map ($CLBP/Magnitude^{ri}_{8,1}$ or $CLBP/Sign^{ri}_{8,1}$) are considered as input of the 5 level Laplacian pyramid decomposition. Then, from each resulted sub-band coefficients we calculated an histogram. Resulting of 4 histograms because the fifth sub-band coefficients is not taken in consideration. Then, from each histogram sub-band coefficients, six statistical features are extracted. Finally, all features are concatenated together into a single ultimate feature vector for classification. Giving a vector length of 4 * 6 = 24 features.

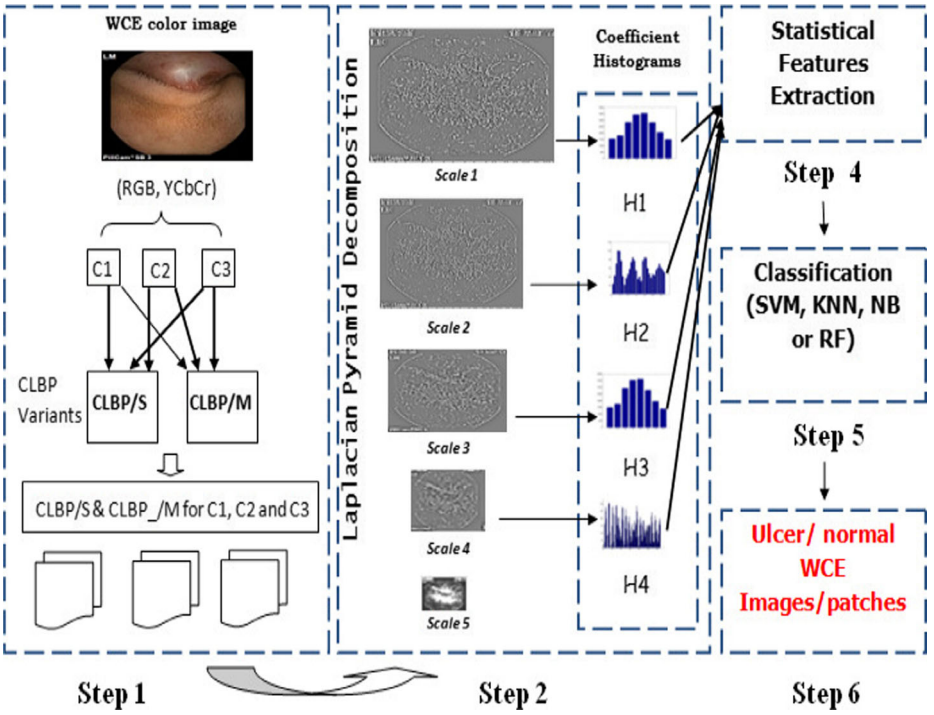

Fig. 2 General diagram of the proposed method

2.2 Brief review of local binary pattern

Local Binary Patterns (LBP) is firstly proposed by Ojala et al. [28] to describe the textures present in gray-scale images. For each pixel in an image, the LBP pattern can be computed by comparing its pixel value with the values of its immediate neighbors. The matrix of weight mask will be used afterwards to code the result of every thresholding [31]. Then, the weighted values are summed and reported in the output image, to correspond the center pixel coordinates in the input image. The LBP operator was extended to a multi-resolution analysis tool, to use any circularly symmetric neighborhoods (P,R) of different sizes. the pair (P,R) means P pixels located on a circle of radius R. In general, the $LBP_{P,R}$ of a pixel (x_c, y_c) is expressed in a decimal form as:

$$LBP_{P,R} = \sum_{p=0}^{P} sign(V_p - V_c)2^P, sign(x) = \begin{cases} 1, & \text{if } x \geq 0 \\ 0, & \text{otherwise} \end{cases} \tag{1}$$

where V_c, V_p are the values of central and neighboring pixels. The original LBP is invariant to monotonic gray scales changes but not invariant to image rotations [8]. To overcome these shortages, the authors of [28] proposed the Rotation Invariant LBP^{ri} and Rotation Invariant Uniform LBP^{riu2} to achieve robustness against image rotation. More details can be found in [28, 35].

2.3 Completed local binary pattern

The completed local binary pattern (CLBP) as an extension to LBP is defined by the local central pixel and the local difference of sign-magnitude transform (LDSMT). The central pixel is defined by a binary global thresholding map named CLBP_C while the LDSMT constitutes of two components, namely: sign component s_p to build the CLBP_S and the magnitude component m_p to build the CLBP_M. The CLBP_S is equivalent to the original LBP. The CLBP_S and CLBP_M can be differently combined to build the final CLBP histograms. The LDSMT is mathematically expressed as given central pixel g_c and gray level of neighboring pixel g_p, p $= \{0, 1, \ldots, P - 1\}$. The local difference is defined as $d_p = (g_p - g_c)$:

$$dp = sp \times mp \qquad \text{and} \qquad \begin{cases} sp = sign(dp) \\ mp = |dp| \end{cases} \tag{2}$$

The local difference vector $[d_0, \ldots, d_{p-1}]$ characterizes the image local structures at g_c. However, different drawbacks are associated. It is sensitive to noise, translation and rotation. To this reason, it is transformed into a sign vector $[s_0, \ldots, s_{p-1}]$ and a magnitude vector $[m_0, \ldots, m_{p-1}]$ to robustly recognize texture patterns. The M component cannot be directly coded as S. In order to make it in a consistent format with that of S, the CLBP_M operator is defined as:

$$CLBP\_M_{P,R} = \sum_{p=0}^{P-1} t(m_p, c)2^p, \qquad t(m_p, c) = \begin{cases} 1, & x \geq c \\ 0, & x < c \end{cases} \tag{3}$$

Where c is the adaptive thresholding. Similarly CLBP_C is computed as:

$$CLBP\_C_{P,R} = t(g_c, C_I) \tag{4}$$

where t is defined in (4) and C_I are the mean of gray values of the whole images. Many variants of CLBP has presented by concatenating the CLBP_M, CLBP_S and CLBP_C

codes mappings, more details can be found in [16]. In our case, to achieve the rotation invariant classification, LBP_M is similar to conventional LBP (LBP_S) that also has $CLBP\_M^{ri}_{P,R}$ variant. Our work is focused on two variants of CLBP denoted $CLBP\_S^{ri}_{P,R}$ and $CLBP\_M^{ri}_{P,R}$.

2.4 Color space

The ulcer abnormality often occurs in association with many diseases, allows it to appear with different color information, white or light-gray color compared with normal mucosa [39]. Processing of both, color and texture, in a suitable model is a complex issue. Till now, it does not remains neither a uniform or credible model for jointing together the color and texture. In regard to previous research, our proposed approach belongs to the strategy where color channels are operated independently [31]. Several works were focused on comparing a variety of color spaces such as RGB, CIELAB, CIEXYZ, YUV, YIQ, CMYK, HSV and HSI to select the most suitable color component for ulcer detection task. Generally, the choice of the color space is done by trial-and-error approachs. Some previous study for ulcer detection like [35, 39], found that RGB and YCbCr color spaces are more suitable to differentiate between ulcer and normal images. These reasons motivates us to use a separate colormaps for each component (R, G and B of RGB color space and Y, Cb and Cr of YCbCr color space). As shown in Fig. 3, the Y component of YCbCr color planes and the G components of RGB color space successfully separate ulcer and normal region. But, we think it's not enough. So, we have to validate this assumption in experiments, to precisely determinate which component are more suitable to our system.

2.5 Multiscale analysis

The work presented in this paper constitutes an extension to our work in [35] which describes a novel multi-scale algorithm that is capable of handling not only the sign

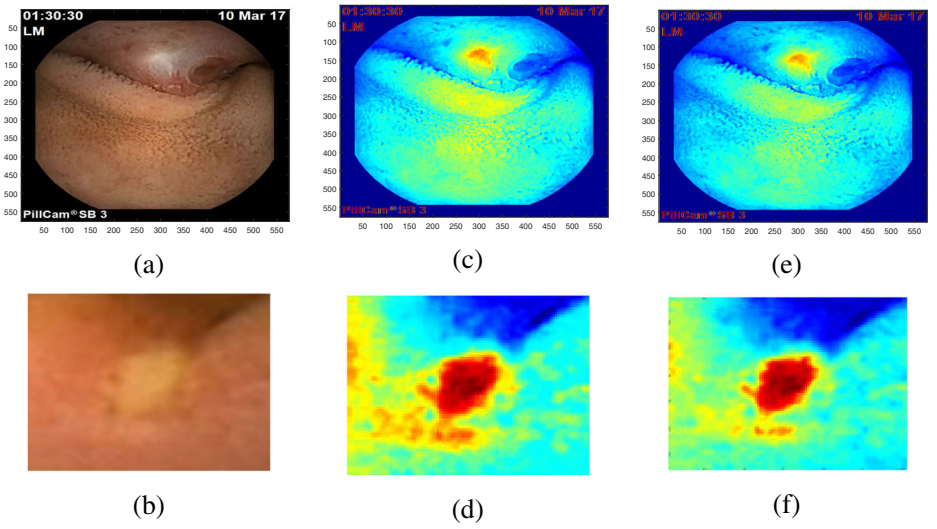

Fig. 3 Ulcerous WCE images and the corresponding different color spaces images. **a**, **b** Original WCE images for the 1^{st} and 2^{nd} databases respectively. **c**, **d** Corresponding images of the second components of the RGB color spaces, and **e**, **f** are the first component for YCbCr color plane for both databases respectively

component of MS-CLBP/S denoted in [35] as (MS_LBP) but also the magnitude component using two datasets.

The extension of the Completed LBP to multi-scale computation (MS-CLBP) can be realized by combining multiple operators at varying parameters (P,R) as stated by many authors [15, 21]. But the most discriminate feature cannot be captured using a single scale since the dominant feature may present at any spatial resolution. Our approach belongs to coarse-to-fine detection strategy (Laplacian pyramid decomposition) as the CLBP descriptor will be more powerful if the image is overpowered by a fine, coarse, directional, or repetitive texture. In this manuscript, we develop a multi-scale representation of two variants of CLBP descriptor (MS-CLBP/Sign and MS-CLBP/Magnitude) to effectively exploit the monochrome and invariant-rotation features at various scales for both databases. Our approach is totally different from The well known multi-scale LBP (MS-LBP) method which lacks a scale-selection mechanism. Unfortunately, the original LBP image suffers from the not invariance to rotation. To increase the discriminative power of the operator, our approach is designed for rotation invariant for both MS-CLBP variants $MS-CLBP/S^{ri}$ and $MS-CLBP/M^{ri}$.

Giving an image with size of $I_x \times I_y$ pixels. Firstly, we calculate the (CLBP/Sign or CLBP/Magnitude) operator of fixed radius R = 1 and number of neighbors P = 8. Secondly, the scales of $I_x \times I_y$ binary strings are obtained by gradually decreasing the (CLBP/S or CLBP/M) map codes at different levels. Precisely, the levels are obtained bit a bit by convolving the lowest level of the (CLBP/S or CLBP/M) code with a low-pass filter, followed by a down sampling method to construct the CLBP Gaussian pyramid version $CLBPG_0, \ldots CLBPG_n$, well-known such as REDUCE operation $CLBPG_k(i, j) = REDUCE(CLBPG_{k-1}(i, j))$. The size of (CLBP/S or CLBP/M) map codes is reduced progressively whenever the level mount up [34]. The superior level of Gaussian pyramid is obtained iteratively from a lowest one, by use of the following equation:

$$CLBPG_k(i, j) = \sum_x \sum_y w(x, y) \times CLBPG_{k-1}(2i + x, 2j + y) \tag{5}$$

Where w(x, y) = w(x) × w(y) is the generated kernel. In each level, we use a low-pass filter and we remove the high frequency part of the image. Consequently, the image becomes progressively blurry. We get the k^{th} level of CLBP Laplacian pyramid version $CLBPL_0, \ldots CLBPL_n$ by up-sampling its $(k + 1)^{th}$ level (known as EXPAND operation), followed by convolution with low-pass filter. Next, subtracting the $(k + 1)^{th}$ level from the k^{th} level of Gaussian pyramid. The equation is given by:

$$CLBPL_k(i, j) = CLBPG_k(i, j) - EXPAND(CLBPG_{k+1}(i, j)) \tag{6}$$

Where the EXPAND operation is described by:

$$CLBPG_{k+1}(i, j) = 4 \sum_x \sum_y w(x, y) * CLBPG_k \left(\frac{i - x}{2}, \frac{j - y}{2} \right) \tag{7}$$

As demonstrated in our previous work [35], 5 level laplacian pyramid decomposition yields to good results. We adopt the same number of decomposition in this paper. So, from each $CLBPL_k$ histogram six statistical features (mean, standard deviation, energy, entropy, skew, kurtosis) are extracted and concatenated together into a ultimate features descriptor. The question is which component(sign or magnitude)is more informative to represent the multi-resolution representation of the WCE images. To answer this question, we experimentally check which operator can efficiency discriminate between normal and abnormal WCE

images for each dataset. From a general viewpoint, the sign component will preserve more image information than the magnitude. In reality, we can't generalize this proposition as textures show a great difference of proprieties. To resolve the matter, the final decision is done based on experiments.

We have to notice, that there exist several multi-scale transforms in the literature, such as steerable pyramids transform, discrete wavelet transform [29], and others. The use of other transformations remains highly feasible.

3 Results and Discussion

3.1 Dataset

For the analysis of the proposed method, we used two dataset; The first dataset used here (Fig. 4), has been acquired with a PillCam SB3 (Cheik Zaid Hospital, Rabat, Morocco) capsule endoscope (see Fig. 1a), with a resolution of 512 × 512 pixels. The dataset comprises a representative set of 240 images (160 normal images and 80 images representing ulcerous regions), obtained from a total of 6 patients (4 normal patients and 2 patients suffering from ulcer). All the images in the dataset have been annotated, precisely and manually,

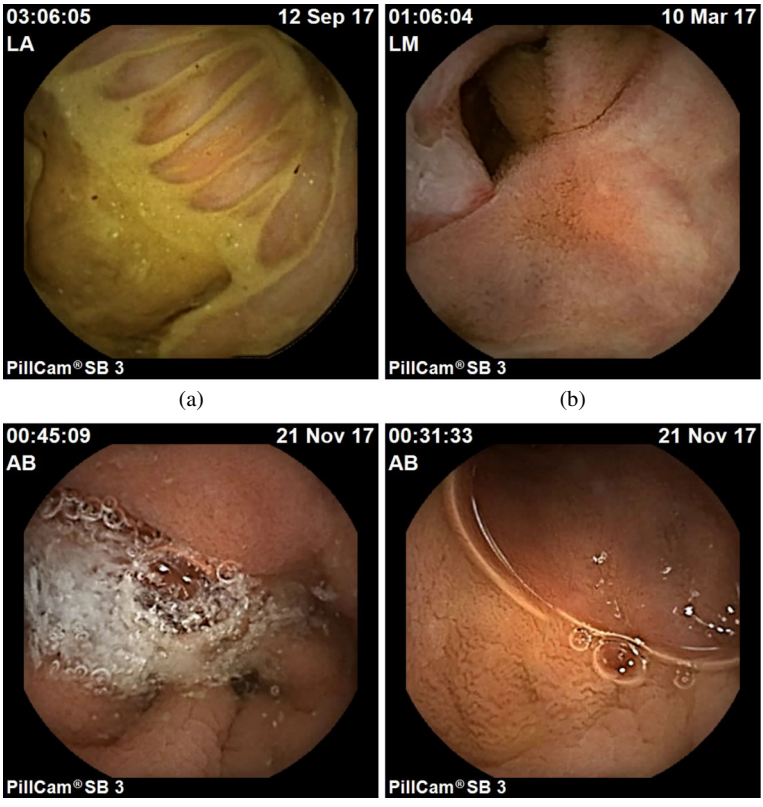

Fig. 4 Example of ulcerous region (**a**, **b**) and normal region (**c**, **d**) of the 1^{st} dataset

by two specialists. The second dataset consists of 133 ulcer and 79 normal WCE patches from the examination data of 20 patients obtained from the authors of [19] according to their agreement. The resolution of the image patches is ranging between 110 × 110 and 160 × 160. The 113 ulcer images were obtained from different ulcer regions to achieve the lowest possible similarity. Furthermore, the normal patches including both simple and confusing healthy tissue (folds, villus, bubbles etc) are used to simulate the actual discrimination process. Three clinicians manually traced the boundaries of the ulcer regions on each single WCE patch and these ulcers annotations served as ground truth. Two experts reviewed the endoscopy video and manually isolated regions of interest (ROI), according to their expertise and upon mutual agreement. Moreover, the ulcer ROIs in this dataset was equally divided into two classes: easy (distinct ulcers of high severity Fig. 5b and hard (hard to detect, low severity ulcers) (Fig. 5a, c). It must be noted that ulcer images were obtained from 100 different events to achieve the lowest possible similarity. Furthermore, normal patches depict both simple and confusing healthy tissue (folds, villus, bubbles etc.) in order to hamper the detection process.

3.2 Evaluation protocol

Many medical diagnosis systems, especially GI tract abnormalities detection researches [9, 18, 37], evaluates the performance of the classifiers in terms of sensitivity, specificity and accuracy. The sensitivity is the ability of a test to correctly identify those with the disease. The specificity is the ability of a test to correctly identify those without the disease. The accuracy represents the ability of a test to correctly differentiate the patient and healthy cases. To estimate the three indexes of a test, we should calculate the number of true positive patterns (TP), the number of false positive patterns (FP), the number of true negative patterns (TN) and the number of false negative patterns (FN). More details can be found in [19, 38].

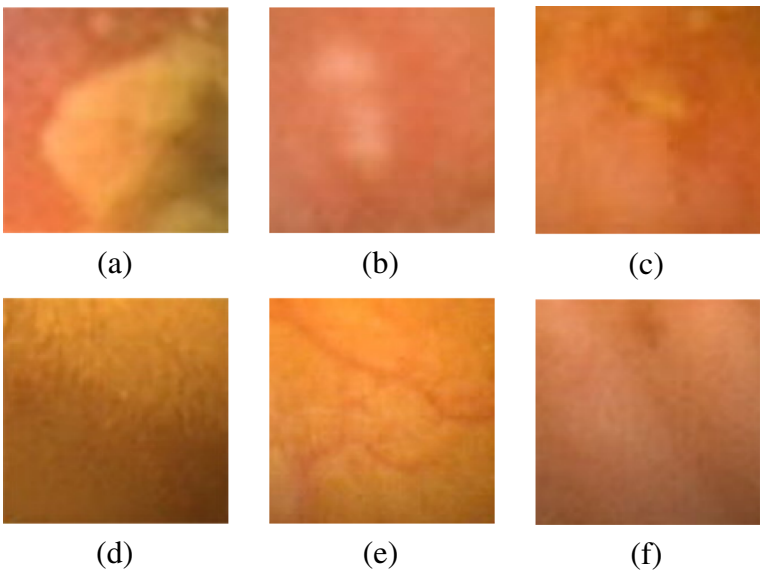

Fig. 5 Example of ulcerous region (**a**, **b** and **c**) and normal region (**d**, **e** and **f**) of the 2^{nd} dataset

Almost, all the abnormality detection methods adopt the accuracy, sensitivity and specificity measures to assess their performance. Those measures are defined as follows:

$$Sensitivity = \frac{\text{Number of correct positive predictions (TP)}}{\text{Number of positives (TP + FN)}} \tag{8}$$

$$Specificity = \frac{\text{Number of correct negative predictions (TN)}}{\text{Number of negatives (TN + FP)}} \tag{9}$$

$$Accuracy = \frac{\text{Number of correct predictions (TP + TN)}}{\text{Total sample (TP + FP + FN + TN)}} \tag{10}$$

We carried out a performance study of five well-known classifiers. Then, we employed the best classifier in term of accuracy as the base classifier to compare the proposed approach with the state-of-art methods. The 5-fold cross validation method [22, 24, 26] was applied to both datasets separately in order to avoid over-fitting. From the total number of images, 80% of them were used for training and the remaining 20% for testing. Then, the mean values of accuracy, sensitivity and specificity indexes were calculated. In our work, we exploit the support vector machine (SVM), multilayer perceptron (MLP), K-nearset neignbor (KNN), Random Forest (RF) and Naive bayes (NB) classifiers and we compare their performances.

3.3 Scale parameter

This work aims to improve the classification performance for normal and ulcerous WCE images for both databases. A 5 level multi-resolution approach based on the completed local binary patterns generates four sub-band coefficients histograms, from the resulted binary map codes as textural image features. The fifth detail of the pyramid is not taken in consideration when calculating the texture feature vector because the pixels of the original image are over enhanced therefore scale distortion on edges. For each coefficients histogram six statistical features are computed that include (mean, standard deviation, entropy, energy, skew and kurtosis). Finally, all sub-band features are concatenated into a final vector features. The process is repeated for each color space channel separately, leading to 24 (6×4) textural features. Based on the results of our previous work [35], four parameters affect the performance of multi-scale method based on completed LBP and laplacian pyramid.

- The P and R: we fixed P = 8 and R = 1.
- The Competed LBP variants: LBP (i.e. CLBP_Sign) or CLBP_Magnitude.
- The Completed LBP mode: $CLBP^{ri}$ fixed to (rotation invariant mode).
- The number of color spaces: RGB, YCbCr.

3.4 Performances evaluation

The evaluation of our model was carried out for both datasets. The multi-scale CLBP/Sign and the multi-scale CLBP/Magnitude were classified separately to evaluate their performance individually in terms of accuracy, sensitivity and specificity using the support vector machine SVM classifier. We used the rotation invariant mode of CLBP with a fixed number of neighbors P = 8 and radius R = 1 as well as two chosen color spaces (RGB and YCBCR) respectively for both databases.

3.4.1 Results of the 1^{st} *dataset*

Figure 6 demonstrates the accuracy rates (%) of the 1^{st} dataset for two multi-scale CLBP variants (MS-CLBP/Sign and MS-CLBP/magnitude). The following remarks can

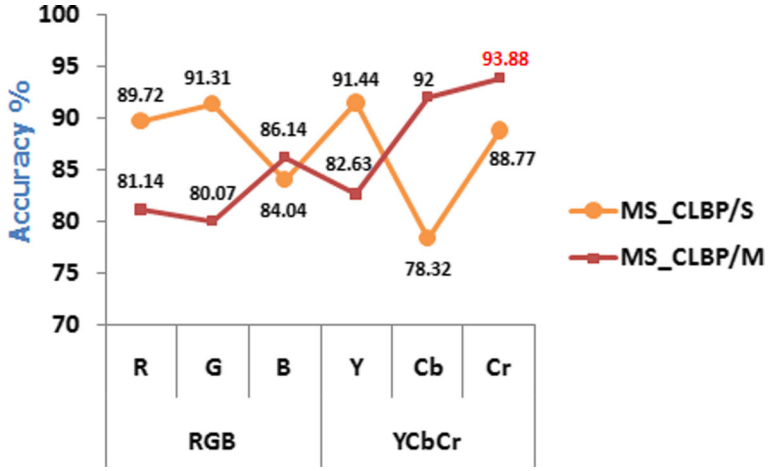

Fig. 6 Semilogy plot of the MS_CLBP variants ($MS\_CLBP/S^{ri}_{(8,1)}$ and $MS\_CLBP/M^{ri}_{(8,1)}$) versus accuracy rate (%) using RGB and YCbCr color spaces for the 1^{st} dataset

be observed. The MS-$CLBP/S^{ri}_{8,1}$ achieved the best classification accuracy of 91.31 and 91.44% using the Green and Y components of RGB and YCbCr color spaces, respectively. The MS-$CLBP/M^{ri}_{8,1}$ achieved the best classification rates of 92 and 93.88% using the Cb and Cr components of YCbCr color space,respectively. In general, the MS-$CLBP/M^{ri}_{8,1}$ operator have exhibited better performance than MS-$CLBP/S^{ri}_{8,1}$ using Cr component of YCbCr color space.

To quantitatively evaluate the performance, we computed the ROC_AUC as shown in Fig. 7. Receiver Operating Characteristics (ROC) is a graphic depiction of the relationship between the true positive ratio (sensitivity) and false positive ratio specificity as a function of the cut-off level of a disease or condition marker. Each point on the ROC curve represents a sensitivity/specificity pair corresponding to a particular decision threshold [11]. A test with perfect discrimination has a ROC curve that passes through the upper left corner (100% sensitivity, 100% specificity). Therefore, the closer the ROC curve is to the upper left corner, the higher the overall accuracy of the test.

The SVM, KNN and Random Forest classifiers must have some parameters to be settled. Therefore, we were first attempted to investigate the best choice of parameter K of KNN, number of trees of Random Forest and the kernel of SVM classifier [23, 25]. We sought to find the optimal value for k-value through quantitative analysis of the model by changing the k-value from 1 to 10. We found K = 3 gives the minimum error. Concerning the Random Forest, we used out-of-bag error rate to determine the number of trees for both databases. We get the minumum out of bag error (OOB) with number of trees equal to 85. Otherwise, for the nonlinear SVM approach, we choose the RBF Kernel trick. This choice was made after a previous study done on our dataset with different kernel tricks (Linear, Polynomial, and Sigmoid). Based on the results of Fig. 7, the 5 fold cross-validation Random Forests and SVM classifiers of the proposed $MS\_CLBP/S^{ri}_{(8,1)}$ method had achieved approximatelyt he same results with an area under curve (ROC) equal to 0.925. The K-Nearest Neighbor shows a very weak AUC value of 0.67. However, Naive Bayes was the classifier which had achieved the lowest area under curve rates with a value of 0.80.

To demonstrate the efficiency of our approach, we conducted a comparison with two methods Color Rotation LBP method [5] and Curvelet based LBP method [18]. Such as,

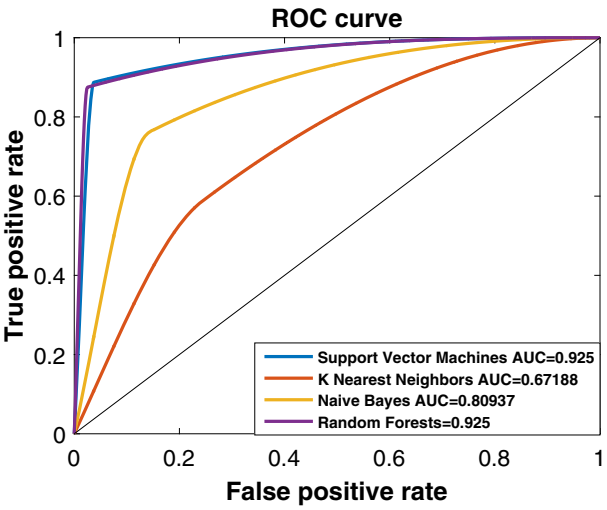

Fig. 7 The receiver operating characteristic (ROC curve) of the $MS\_CLBP/M^{ri}_{(8,1)}$ for the 1^{st} dataset

these two approaches show an improvement of the original LBP descriptor for WCE ulcer abnormality detection. Table 1 indicates the main accuracy, sensitivity and specificity of 5-fold cross validation of the competitor methods as well as the proposed method $MS-CLBP/M^{ri}_{8,1}$, giving a higher result on the 1^{st} dataset using the Cr component of YCbCr color space as demonstrated in Fig. 6. We implemented the state-of-art methods [5, 18] using the same parameters as stated in their original papers. All the approaches have been tested on the same data using the 5-fold cross validation for both SVM (RBF kernel) and Random forest classifiers.

Based on experiments of the 1^{st} dataset, the MS-$CLBP/M^{ri}_{8,1}$ using the Cr component of YCbCr color space shows a superior performance with an improvement of 10.68, 8.47% in accuracy, 2.73 and 2.65% in term of sensitivity respectively compared with the state-of-the-art methods for the SVM classifier. Also, the Random Forest classifier shows an improvement of 6.98, 8.97% in accuracy, 2.6 and 0.29% in term of sensitivity compared with these two methods. This result validates that the proposed system possesses superior ability to characterize the WCE images and demonstrates good discriminative capability for ulcer detection.

Table 1 5-fold cross validation of Performance Comparison of Ulcer Diagnosis Methods for 1^{st} dataset

Performance %	CLBP [18]	CR_ULBP [5]	MS-CLBP/M
SVM classifier			
Accuracy	83.2	85.41	93.88
Sensitivity	94.48	94.56	97.21
Specificity	60.64	67.12	87.22
RF classifier			
Accuracy	85.78	83.79	92.76
Sensitivity	95.13	92.82	95.42
Specificity	67.08	65.75	87.43

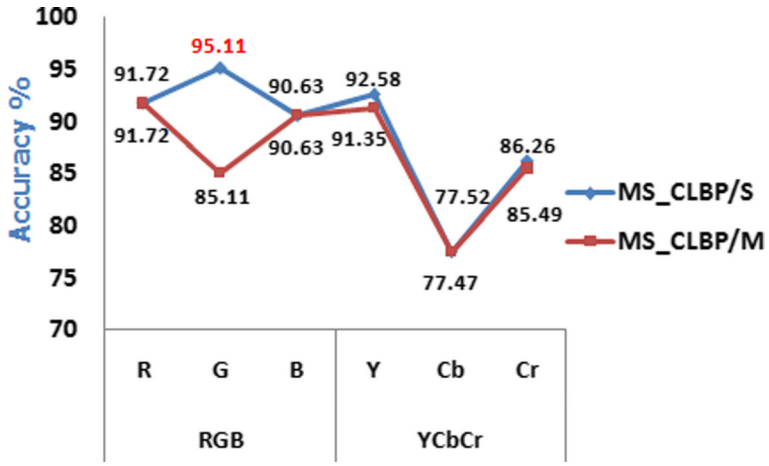

Fig. 8 Semilogy plot of the MS_CLBP variants ($MS\_CLBP/S^{ri}_{(8,1)}$ and $MS\_CLBP/M^{ri}_{(8,1)}$) versus accuracy rate (%) using RGB and YCbCr color spaces for the 2^{nd} dataset

3.4.2 Results of the 2^{nd} dataset

Figure 8 shows the accuracy rate in percentage (%) of the second dataset using two CLBP variants (CLBP/S, CLBP/M). As shown in Fig. 8, the MS-$CLBP/S^{ri}_{8,1}$ operator outperforms the MS-$CLBP/M^{ri}_{8,1}$ in case of RGB color space. While, they have approximately equal results in case of YCbCr color space. The system performance has achieved maximum accuracy rate of 95.11% in the case of MS-$CLBP/S^{ri}_{8,1}$ using the G component of RGB color space.

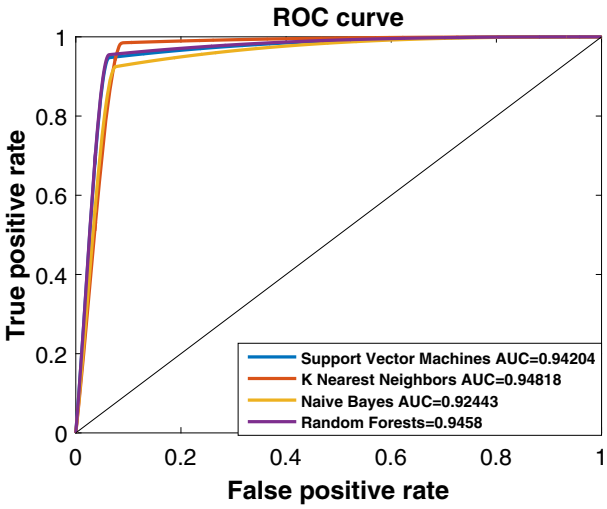

Fig. 9 The Receiver Operating Characteristic (ROC curve) of the $MS\_CLBP/S^{ri}_{(8,1)}$ for the 2^{nd} dataset

The optimal value of K of KNN for the 2^{nd} dataset equal to 2. Concerning the Random Forest, we get the minumum out of bag error (OOB) with number of trees equal to 20. Otherwise, for the nonlinear SVM approach, we choose the RBF Kernel trick. Based on the results of Fig. 9, the 5 fold cross-validation random forest classifier, SVM and K Nearest Neighbors classifiers had achieved the best performance among the different classifiers evaluated with an area under curve (ROC) approximately equal to 0.94 for the 2^{nd} dataset. However, Naive Bayes was the classifier which had achieved the lowest area under curve rates with a value of 0.92.

Like the 1^{st} dataset, we conduct a comparison of the 2^{nd} dataset including patches with the same state-of-the-art method [5, 18], using the 5-fold cross validation of the SVM (RBF kenel) and Random Forests classifiers. The performance comparison results is reported in Table 2. This table demonstrates that the $MS-CLBP/S^{ri}_{8,1}$ shows an encouraging performance using Green component of RGB color space and SVM classifier with a gain of 12.73, 13.54% in accuracy, 12.77, 6.17% in sensitivity compared with the state-of-the-art methods, respectively. Also, the result of Random Forests classifier shows an improvement of 15.43, 7.13% in term of accuracy and 13.81, 4.72% in term of sensitivity. The results turns out that the proposed method outperforms other two compared methods in terms of accuracy and sensitivity.

3.5 Computational complexity

The computational complexity of the proposed method depends on the size of the original images, number of neignbors P and radius R during CLBP computation, number of levels of laplacian pyramid decomposition, number of extracted features and K-fold validation of the classifiers . Tests were conducted on a PC running Windows, featuring an Intel(R) Xeon(R) CPU running at 2.83 Ghz with 8GB of RAM, using Matlab Version R2015b. Table 3 summarizes the most computationally functions within the implementation of the approach. Processing times have been normalized on image from the 1st dataset with a resolution of 576 × 576. The functions listed in the table constitute 90% of total execution time. Sequences 1-6 are executed once for each image. Whereas, sequences 7-8 execute a loop 5 times per image. As shown in Table 3, Completed LBP exhibits a high computational running time compared with the other functions. We apply the same process to 4 images of sizes (576 × 576 pixels) taken from the 1^{st} dataset, and 4 patches of sizes (80 × 80, 128 × 128, 64 × 64, 128 × 128 pixels) taken from the 2^{nd} dataset. Finally, we take the average of total execution times as the running time for each image. Considering the 1^{st} dataset, the

Table 2 5-fold cross validation of Performance Comparison of Ulcer Diagnosis Methods for 2^{nd} dataset

Performance %	CLBP [18]	CR_ULBP [5]	MS-CLBP/S
SVM classifier			
Accuracy	77.78	90.01	95.11
Sensitivity	59.5	94.2	95.64
Specificity	88.37	87.61	94.83
RF classifier			
Accuracy	81.08	89.38	96.51
Sensitivity	83.54	92.63	97.35
Specificity	79.64	87.52	96.04

Table 3 5-fold cross validation of Performance Comparison of Ulcer Diagnosis Methods for 2^{nd} dataset

Sequence	Function name	Normalized exec. time (s)
1	read_picture_file	0.052
2	color_space_conversion	0.029
3	component_separation	0.021
4	build_CLBP	0.453
5	Laplacian_Pyramid_Decomposition	0.261
6	features_extraction	0.274
7	K-fold_SVM_Model	0.203
8	picture_prediction	0.041

average computational execution times of the 4 images is 1.393 secondes. Wheares, the average computational execution times of the 4 patches for the 2^{nd} dataset is 0.455 secondes.

4 Conclusion

In this paper, we proposed a new computer-aided detection system to detect ulcer from WCE images. The performance of multi-resolution approach based on Completed LBP and laplacian pyramid shows its effectiveness when compared to the state of art methods. This may be explained by the fact that the approach takes in consideration the scale, orientation and color information. We conducted several experiments to compare the CLBP variants (sign and magnitude components) using each component of RGB and YCBCR color spaces. Based on the experiments of the first dataset, the MS_CLBP/Magnitude achieve a promising results using the Cr component of YCbCr color space. Whereas, the MS_CLBP/Sign method achieves a high performance for the second dataset using the Green component of RGB color space. In the future work, we will use other kind of features to robustly discriminate ulcer mucosa from the normal ones. Thus, we will try some improved feature selection methods like PCA and optimizing various parameters to achieve further improvements.

Acknowledgements The authors would like to thank the Cheik Zaid Hospital for sharing the WCE images. In addition, the authors would like to acknowledge and thank Dr. Meryem BENNANI, the responsible of the gastroenterology department, and Dr. Hasnae AHENDAR for their assistance and technical comments, as well as their professional suggestions during the preparation of the dataset.

Compliance with Ethical Standards

Conflict of interests The authors declare that they have no conflict of interest.

References

1. Charfi S, El Ansari M (2017) Computer-aided diagnosis system for ulcer detection in wireless capsule endoscopy videos. In: 2017 international conference on advanced technologies for signal and image processing (ATSIP). IEEE, pp 1–5
2. Charfi S, El Ansari M (2017) Gastrointestinal tract bleeding detection from wireless capsule endoscopy videos. In: Proceedings of the second international conference on internet of things and cloud computing. ACM, p 111

3. Charfi S, El Ansari M (2018) Computer-aided diagnosis system for colon abnormalities detection in wireless capsule endoscopy images. Multimedia Tools and Applications 77(3):4047–4064. Springer
4. Charisis V, Hadjileontiadis L, Sergiadis G (2012) Enhanced ulcer recognition from capsule endoscopic images using texture analysis. In: New advances in the basic and clinical gastroenterology. InTech
5. Charisis VS, Katsimerou C, Hadjileontiadis LJ, Liatsos CN, Sergiadis GD (2013) Computer-aided capsule endoscopy images evaluation based on color rotation and texture features: an educational tool to physicians. In: 2013 IEEE 26th international symposium on computer-based medical systems (CBMS). IEEE, pp 203–208
6. Chen Y, Lee J (2012) Ulcer detection in wireless capsule endoscopy video. In: Proceedings of the 20th ACM international conference on multimedia. ACM, pp 1181–1184
7. Cortes C, Vapnik V (1995) Support vector machine. Mach Learn 20(3):273–297
8. Davarpanah SH, Khalid F, Abdullah LN, Golchin M (2016) A texture descriptor: background local binary pattern (bglbp). Multimedia Tools and Applications 75(11):6549–6568
9. Eid A, Charisis VS, Hadjileontiadis LJ, Sergiadis GD (2013) A curvelet-based lacunarity approach for ulcer detection from wireless capsule endoscopy images. In: 2013 IEEE 26th international symposium on computer-based medical systems (CBMS). IEEE, pp 273–278
10. El Ansari M, Charfi S (2017) Computer-aided system for polyp detection in wireless capsule endoscopy images. In: 2017 international conference on wireless networks and mobile communications (WINCOM). IEEE, pp 1–6
11. El Ansari M, Lahmyed R, Trémeau A (2018) A hybrid pedestrian detection system based on visible images and LIDAR data. In: Proceedings of the 13th international joint conference on computer vision, imaging and computer graphics theory and applications (VISIGRAPP 2018) - Volume 5: VISAPP, Funchal, Madeira, Portugal, January 27–29, 2018, pp 325–334
12. Ellahyani A, El Ansari M (2017) Mean shift and log-polar transform for road sign detection. Multimedia Tools and Applications 76(22):24495–24513. Springer
13. Ershad SF (2012) Texture classification approach based on combination of edge & co-occurrence and local binary pattern. arXiv:12034855
14. Gan T, Wu JC, Rao NN, Chen T, Liu B (2008) A feasibility trial of computer-aided diagnosis for enteric lesions in capsule endoscopy. World Journal of Gastroenterology: WJG 14(45):6929
15. Guo Z, Zhang L, Zhang D, Mou X (2010) Hierarchical multiscale lbp for face and palmprint recognition. In: 2010 17th IEEE international conference on image processing (ICIP). IEEE, pp 4521–4524
16. Guo Z, Zhang L, Zhang D (2010) A completed modeling of local binary pattern operator for texture classification. IEEE Trans Image Process 19(6):1657–1663. IEEE
17. Htwe TM, Shen W, Li L, Poh CK, Liu J, Lim JH, Ong EH, Ho KY (2010) Adaboost learning for small ulcer detection from wireless capsule endoscopy (wce) images. In: Asia Pacific signal and information processing association (APSIPA) conference
18. Li B, Meng MQH (2009) Texture analysis for ulcer detection in capsule endoscopy images. Image Vis Comput 27(9):1336–1342
19. Li B, Meng MQH, Lau JY (2011) Computer-aided small bowel tumor detection for capsule endoscopy. Artif Intell Med 52(1):11–16
20. Liaw A, Wiener M et al (2002) Classification and regression by randomforest. R News 2(3):18–22
21. Lin Q, Qi W (2015) Multi-scale local binary patterns based on path integral for texture classification. In: 2015 IEEE international conference on image processing (ICIP). IEEE, pp 26–30
22. Liu Y, Cui J, Zhao H, Zha H (2012) Fusion of low-and high-dimensional approaches by trackers sampling for generic human motion tracking. In: 2012 21st international conference on pattern recognition (ICPR). IEEE, pp 898–901
23. Liu Y, Nie L, Han L, Zhang L, Rosenblum DS (2015) Action2activity: recognizing complex activities from sensor data. In: IJCAI, vol 2015, pp 1617–1623
24. Liu L, Cheng L, Liu Y, Jia Y, Rosenblum DS (2016) Recognizing complex activities by a probabilistic interval-based model. In: AAAI, vol 30, pp 1266–1272
25. Liu Y, Nie L, Liu L, Rosenblum DS (2016) From action to activity: sensor-based activity recognition. Neurocomputing 181:108–115
26. Liu Y, Zhang L, Nie L, Yan Y, Rosenblum DS (2016) Fortune teller: predicting your career path. In: AAAI, vol 2016, pp 201–207
27. Nawarathna R, Oh J, Muthukudage J, Tavanapong W, Wong J, De Groen PC, Tang SJ (2014) Abnormal image detection in endoscopy videos using a filter bank and local binary patterns. Neurocomputing 144:70–91
28. Ojala T, Pietikainen M, Maenpaa T (2002) Multiresolution gray-scale and rotation invariant texture classification with local binary patterns. IEEE Trans Pattern Anal Mach Intell 24(7):971–987

29. Omidyeganeh M, Ghaemmaghami S, Shirmohammadi S (2013) Application of 3d-wavelet statistics to video analysis. Multimedia Tools and Applications 65(3):441–465
30. Peterson LE (2009) K-nearest neighbor. Scholarpedia 4(2):1883
31. Porebski A, Vandenbroucke N, Macaire L (2008) Haralick feature extraction from lbp images for color texture classification. In: First workshops on image processing theory, tools and applications. 2008. IPTA 2008. IEEE, pp 1–8
32. Salehpour P, Bahar HB, Karimian G, Ebrahimnezhad H (2016) Adapted bit-plane probability and wavelet-based ulcer detection in wireless capsule endoscopy images. Biomedical Engineering: Applications, Basis and Communications 28(04):1650,029
33. Seguí S, Drozdzal M, Pascual G, Radeva P, Malagelada C, Azpiroz F, Vitrià J (2016) Generic feature learning for wireless capsule endoscopy analysis. Comput Biol Med 79:163–172
34. Simoncelli EP, Freeman WT (1995) The steerable pyramid: a flexible architecture for multi-scale derivative computation. In: International conference on image processing, 1995. Proceedings, vol 3. IEEE, pp 444–447
35. Souaidi M, Ait Abdelouahad A, El Ansari M (2017) A fully automated ulcer detection system for wireless capsule endoscopy images. In: 3th international conference on advanced technologies for signal and image processing (ATSIP'2017), proceeding under publication. IEEE
36. Szczypiński P, Klepaczko A, Pazurek M, Daniel P (2014) Texture and color based image segmentation and pathology detection in capsule endoscopy videos. Comput Methods Prog Biomed 113(1):396–411
37. Yeh JY, Wu TH, Tsai WJ (2014) Bleeding and ulcer detection using wireless capsule endoscopy images. J Softw Eng Appl 7(05):422
38. Yu L, Yuen PC, Lai J (2012) Ulcer detection in wireless capsule endoscopy images. In: 2012 21st international conference on pattern recognition (ICPR). IEEE, pp 45–48
39. Yuan Y, Wang J, Li B, Meng MQH (2015) Saliency based ulcer detection for wireless capsule endoscopy diagnosis. IEEE Trans Med Imaging 34(10):2046–2057
40. Zhang G, Wang W, Shin S, Hruska CB, Son SH (2015) Fourier irregularity index: a new approach to measure tumor mass irregularity in breast mammogram images. Multimedia Tools and Applications 74(11):3783–3798

Meryem Souaidi received his Master degree in distributed systems from The University of Ibn Zohr, Agadir 2015. He is currently pursuing the Ph.D. degree in computer science at Ibn Zohr University, Faculty of Sciences, Agadir - Morocco. His research interests include medical image analysis, image processing, and computer vision.

Abdelkaher Ait Abdelouahed received the PhD from the University of Mohammed V-Agdal in 2013. Currently, he is an assistant professor at University of Agadir. His research focuses on the image quality assessment area.

Mohamed El Ansari received the M.S. and PhD degrees in computer science from Sidi Mohamed Ben Abdellah University, Fez - Morocco, in 1995 and 2000, respectively. He was a post-doctoral fellowship at ENSEIRB (École Nationale Supérieure d'Electronique, Informatique, Télécommunications, Mathématique et Mécanique de Bordeaux), France, from 2001 to 2002. He was also an ERCIM (European Research Consortium for Informatics and Mathematics) post-doctoral fellowship at NTNU (Norges Teknisk-Naturvitenskapelige Universitet - Norwegian University of Science and Technology), Norway, from 2002 to 2003. He was appointed as assistant professor at University of Ibn Zohr, Agadir, Morocco, where he was promoted as full professor in 2015. He served as visiting professor at INSA (Institut National des Sciences Appliquées, 2007–2009) of Rouen, France, Ecole Centrale de Nantes (2011–2012), France, and University Jean Monnet (2013–2014), Saint-Etienne, France. He was a visiting Fullbright Scholar at the University of Nevada, Reno (UNR), USA in 2010. His research interests include image processing and computer vision. Apart from his experience with teaching and working with researchers from different countries, he published and served as a reviewer at numerous international conferences and journals.